AAS 25-582

DISCRETE PARAMETER FLOW FILTERING FOR SPARSE TRACKING OF OBJECTS IN CISLUNAR ORBITS

William N. Fife[*], Kyle J. DeMars[†], and Gunner S. Fritsch[‡]

Numerous challenges exist when conducting recursive Bayesian inference for nonlinear systems—especially when observations are sparsely available. Although increasing the amount of available data to process is tempting, it is simply a reality that more sophisticated algorithms are required to track the rapidly increasing number of space objects. To that end, this work develops a discrete homotopic continuation of Bayes' rule that partitions the traditional single-step update into multiple incremental updates. The method, termed discrete parameter flow, is applied with Gaussian mixture representations to achieve superior performance compared to traditional filtering schemes on a cislunar object tracking application. Multiple variations of the filter are presented including a square-root factorized version and a novel adaptive-inference-step procedure that reduces the computational requirements of discrete parameter flow without sacrificing performance.

INTRODUCTION

The precise estimation of a spacecraft's state (e.g., position and velocity) is of crucial importance for space domain awareness and mission operations. Almost all spacecraft in the cislunar regime use observations from an increasingly constrained set of ground-based assets to determine an updated estimate of the spacecraft's state. These assets are tasked with tracking not only cislunar objects, but Earth-orbiting satellites and orbital debris[1]. Moreover, the cislunar regime introduces non-Keplerian dynamics that can lead to a loss of custody for significant time intervals between measurements. This puts an imperative for tracking algorithms—the concern of this work—to "do more with less" as the problem cannot be overcome with an ever-increasing number of sensors.

Conventional tracking algorithms take a given estimate and uncertainty (e.g., from initial orbit determination or prior tracking) and leverage the underlying dynamics to evolve the estimate and uncertainty to a measurement epoch. At the epoch, the measurement is processed, typically via an approximation of Bayes' rule, to arrive at an updated estimate and uncertainty. The process is repeated for the next measurement epoch and thus aptly named recursive Bayesian inference[2]. It is ubiquitous for the inference phase to be conducted in "one step"; that is, the measurement information is incorporated into the state and its uncertainty at once. Alternatively, this work develops a partitioned solution of the inference phase through a homotopic continuation of Bayes' rule. The underlying motivation for this partitioned approach is that errors arising from linearization (either analytical or statistical) can be ameliorated through "smaller" linearization steps.

Iterative or progressive inference procedures have been investigated previously. The progressive Bayes framework[3] introduced the idea of approaching the true posterior density via intermediate

[*]PhD Candidate, Department of Aerospace Engineering, Texas A&M University, College Station, TX.
[†]Associate Professor, Department of Aerospace Engineering, Texas A&M University, College Station, TX.
[‡]Sr. Professional Staff I , SES/SAC , Johns Hopkins University Applied Physics Laboratory, Laurel, MD.

densities. Instead of partitioning Bayes' rule, the authors of Reference 3 form an ordinary differential equation (ODE) for the parameters of an approximating distribution where the ODE is associated with the minimization of a performance index. Another approach is particle flow[4,5] wherein Bayes' rule is transformed into a linear-log homotopy and used to flow particle representations of the prior toward the posterior. The recursive update by Zanetti[6] splits the Kalman gain equation into equal partitions in order to re-linearize the measurement model. Michaelson et al.[7,8] introduced partitioning of the measurement likelihood as is conducted in the approach proposed herein, but limited their developments to Gaussian densities or particle representations. Lastly, the work by Craft[9] provides a continuous flow of parameters (e.g., Gaussian mixture components) through the inference step that is general to multiple types of likelihoods. The current work is distinct from Reference 9 in two ways. Firstly, for computational expediency and runtime guarantee, this work retains the finite iterative inference procedure instead of a numerical integration. Secondly, a method for adaptively selecting the size of discrete inference steps is presented.

This work is organized as follows. First, the recursive Bayesian inference paradigm is outlined and a description of the recursion of partial updates is given for various filter implementations. A method for selecting the discrete inference steps is also described. Then, a low-dimensional example is provided to illustrate the benefits of this approach. Additionally, a cislunar tracking scenario is presented along with conclusions on those results.

DISCRETE PARAMETER FLOW FILTERING

Consider the system state vector $\boldsymbol{x}_k \in \mathbb{R}^n$ at time t_k that evolves and is observed via the discrete, nonlinear stochastic processes

$$\boldsymbol{x}_k = \boldsymbol{f}(\boldsymbol{x}_{k-1}) + \boldsymbol{w}_{k-1} \tag{1a}$$

$$\boldsymbol{z}_k = \boldsymbol{h}(\boldsymbol{x}_k) + \boldsymbol{v}_k \,, \tag{1b}$$

where $\boldsymbol{f}(\cdot)$ represents the system dynamics, $\boldsymbol{h}(\cdot)$ is the observation model, $\boldsymbol{z}_k \in \mathbb{R}^m$ is the measurement, and $\boldsymbol{w}_{k-1}$ and $\boldsymbol{v}_k$ are noise vectors with covariances $\boldsymbol{P}_{ww}$ and $\boldsymbol{P}_{vv}$, respectively. At an initial epoch t_0, it is assumed that all possible configurations of the state are characterized by a probability density function (pdf) $p(\boldsymbol{x}_0)$. This work is concerned with the Bayesian filtering recursion comprised of two stages—predictor and corrector. Since particular focus is given to the corrector, only a brief overview of the predictor stage is given. For two arbitrary epochs t_{k-1} and t_k, the predictor is given by the Chapman-Kolmogorov equation[10] as

$$p(\boldsymbol{x}_k \mid \boldsymbol{z}_{1:k-1}) = \int_{\mathbb{R}^n} p(\boldsymbol{x}_k \mid \boldsymbol{x}_{k-1}) p(\boldsymbol{x}_{k-1} \mid \boldsymbol{z}_{1:k-1}) \mathrm{d}\boldsymbol{x}_{k-1} \,, \tag{2}$$

where $p(\boldsymbol{x}_k \mid \boldsymbol{z}_{1:k-1})$ is the prior pdf, $p(\boldsymbol{x}_k \mid \boldsymbol{x}_{k-1})$ is termed the transition pdf, and $p(\boldsymbol{x}_{k-1} \mid \boldsymbol{z}_{1:k-1})$ is the posterior state pdf at t_{k-1} conditioned on all past measurements (i.e., $\boldsymbol{z}_{1:k-1} = \{\boldsymbol{z}_1, \ldots, \boldsymbol{z}_{k-1}\}$). In most practical cases, Equation (2) is intractable in the given form due to a lack of conjugacy between the pdfs and/or inability to represent the pdfs via finite parameters. Thus, it is common to choose a parameterized density model (e.g., Gaussian mixtures) and approximate Equation (2) through linearization, quadrature, or Monte Carlo techniques[11].

Corrector

Let the representation of choice for the state pdf be a Gaussian mixture model (GMM); as such, the prior pdf is an L_x-component mixture of the form

$$p(\boldsymbol{x}_k) = \sum_{\ell=1}^{L_x} w_{x,k}^{(\ell)-} p_g(\boldsymbol{x}_k; \boldsymbol{m}_{x,k}^{(\ell)-}, \boldsymbol{P}_{xx,k}^{(\ell)-}) \,, \tag{3}$$

where $p_g(\boldsymbol{y}; \boldsymbol{m}_y, \boldsymbol{P}_{yy})$ is a multivariate Gaussian pdf with mean $\boldsymbol{m}_y$ and covariance $\boldsymbol{P}_{yy}$. The weights, means, and covariances of each component within the mixture are $w_x^{(\ell)-}$, $\boldsymbol{m}_{x,k}^{(\ell)-}$, and $\boldsymbol{P}_{xx,k}^{(\ell)-}$, respectively. The conditional dependence on past measurements $\boldsymbol{z}_{1:k-1}$ is dropped on the left-hand side of Equation (3) for notational convenience. Note that a singular Gaussian representation of the prior, and thus a Gaussian form of discrete parameter flow, is a special case of the GMM form where $L_x = 1$ and $w_x^{(1)-} = 1$. The corrector is given by Bayes' rule, defined as

$$p(\boldsymbol{x}_k \mid \boldsymbol{z}_k) = \frac{1}{p(\boldsymbol{z}_k)} p(\boldsymbol{z}_k \mid \boldsymbol{x}_k) p(\boldsymbol{x}_k) \,, \tag{4}$$

where $p(\boldsymbol{z}_k \mid \boldsymbol{x}_k)$ is the likelihood density. For measurement models given by Equation (1b), approximations—of similar type to those used on Equation (2)—must be made to facilitate solutions to Bayes' rule. However, it is common to evaluate Equation (4) in "one step" as is done in Reference 12.

Alternatively, consider a partitioning of the corrector that progressively incorporates measurement information as follows. Let a sequence of points $s_m \in [0, 1]$ be prescribed such that $0 = s_1 < s_2 < \cdots < s_{M+1} = 1$ and $\sum_m \Delta s_m = 1$ where $\Delta s_m = s_{m+1} - s_m$. The likelihood can then be equivalently expressed as

$$p(\boldsymbol{z}_k \mid \boldsymbol{x}_k) = \prod_{m=1}^{M} p^{\Delta s_m}(\boldsymbol{z}_k \mid \boldsymbol{x}_k) \,. \tag{5}$$

Let the likelihood be given by the Gaussian pdf $p_g(\boldsymbol{z}_k; \boldsymbol{h}(\boldsymbol{x}_k), \boldsymbol{P}_{vv})$, which is the probabilistic state space model of Equation (1b), assuming that the measurement noise is zero-mean and Gaussian with covariance $\boldsymbol{P}_{vv}$. Substituting the Gaussian likelihood into Equation (5) gives

$$p(\boldsymbol{z}_k \mid \boldsymbol{x}_k) = |2\pi \boldsymbol{P}_{vv}|^{-\frac{1}{2}} \prod_{m=1}^{M} |2\pi \boldsymbol{P}_{vv}/\Delta s_m|^{\frac{1}{2}} \times p_g(\boldsymbol{z}; \boldsymbol{h}(\boldsymbol{x}_k), \boldsymbol{P}_{vv}/\Delta s_m) \,. \tag{6}$$

Note that, since $\Delta s_m > 0$, there are no (theoretical) issues with the singularity of $(\boldsymbol{P}_{vv}/\Delta s_m)$ so long as $\boldsymbol{P}_{vv}$ is nonsingular. Substituting Equations (3) and (6) into Equation (4) yields

$$\begin{aligned} p(\boldsymbol{x}_k | \boldsymbol{z}_k) \propto \sum_{\ell=1}^{L_x} w_x^{(\ell)-} |2\pi \boldsymbol{P}_{vv}{}^{-\frac{1}{2}} \left[\prod_{k=1}^{M} |2\pi \boldsymbol{P}_{vv}/\Delta s_k{}^{\frac{1}{2}} \right] \\ \times \left[\prod_{k=1}^{M} p_g(\boldsymbol{z}; \boldsymbol{h}(\boldsymbol{x}), \boldsymbol{P}_{vv}/\Delta s_m) \right] p_g(\boldsymbol{x}; \boldsymbol{m}_{x,k}^{(\ell)-}, \boldsymbol{P}_{xx,k}^{(\ell)-}) \,, \end{aligned}$$

where proportionality of Bayes' rule is not enforced for brevity. Applying a generalized form of the

Ho-Lee equation[13] for the products of Gaussians in conjunction with statistical linearization of the measurement model, the resulting posterior pdf is a GMM given by

$$p(\boldsymbol{x}_k \mid \boldsymbol{z}_k) = \sum_{\ell=1}^{L_x} w_{x_k}^{(\ell)+} p_g(\boldsymbol{x}_k; \boldsymbol{m}_{x,k}^{(\ell)+}, \boldsymbol{P}_{xx,k}^{(\ell)+}) \,,$$

where the weights, means, and covariances are determined by the iterative relationships

$$w_x^{(\ell,i)} = k^{(\ell,i)} w_x^{(\ell,i-1)} \,/\, \textstyle\sum_{\ell'=1}^{L_x} k^{(\ell',i)} w_x^{(\ell',i-1)} \tag{7a}$$

$$\boldsymbol{m}_x^{(\ell,i)} = \boldsymbol{m}_x^{(\ell,i-1)} + \boldsymbol{K}^{(\ell,i)} (\boldsymbol{z} - \boldsymbol{m}_h^{(\ell,i-1)}) \tag{7b}$$

$$\boldsymbol{P}_{xx}^{(\ell,i)} = \boldsymbol{P}_{xx}^{(\ell,i-1)} - \boldsymbol{K}^{(\ell,i)} \boldsymbol{P}_{hh}^{(\ell,i-1)} (\boldsymbol{K}^{(\ell,i)})^T - \boldsymbol{K}^{(\ell,i)} (\boldsymbol{P}_{vv}/\Delta s_i) (\boldsymbol{K}^{(\ell,i)})^T \,, \tag{7c}$$

which are applied for $1 \leq i \leq M$. This iterative procedure is initialized with $w_x^{(\ell,0)} = w_{x,k}^{(\ell)-}$, $\boldsymbol{m}_x^{(\ell,0)} = \boldsymbol{m}_{x,k}^{(\ell)-}$ and $\boldsymbol{P}_{xx}^{(\ell,0)} = \boldsymbol{P}_{xx,k}^{(\ell)-}$. When the last iteration is completed, the output is $w_{x,k}^{(\ell)+} = w_x^{(\ell,M)}$, $\boldsymbol{m}_{x,k}^{(\ell)+} = \boldsymbol{m}_x^{(\ell,M)}$ and $\boldsymbol{P}_{xx,k}^{(\ell)+} = \boldsymbol{P}_{xx}^{(\ell,M)}$. The weight and state gains that appear in Equations (7) are given by

$$k^{(\ell,i)} = p_g(\boldsymbol{z}; \boldsymbol{m}_h^{(\ell,i-1)}, \boldsymbol{P}_{hh}^{(\ell,i-1)} + \boldsymbol{P}_{vv}/\Delta s_i) \tag{8a}$$

$$\boldsymbol{K}^{(\ell,i)} = \boldsymbol{P}_{xh}^{(\ell,i-1)} (\boldsymbol{P}_{hh}^{(\ell,i-1)} + \boldsymbol{P}_{vv}/\Delta s_i)^{-1} \,, \tag{8b}$$

and the mean, cross-covariance (with the state) and covariance of the nonlinear function $\boldsymbol{h}(\boldsymbol{x})$ that are required to complete each iteration are defined in terms of expected values as

$$\boldsymbol{m}_h^{(\ell,\cdot)} = \mathbb{E}\{\boldsymbol{h}(\boldsymbol{x})\} \tag{9a}$$

$$\boldsymbol{P}_{xh}^{(\ell,\cdot)} = \mathbb{E}\{(\boldsymbol{x} - \boldsymbol{m}_x^{(\ell,\cdot)})(\boldsymbol{h}(\boldsymbol{x}) - \boldsymbol{m}_h^{(\ell,\cdot)})^T\} \tag{9b}$$

$$\boldsymbol{P}_{hh}^{(\ell,\cdot)} = \mathbb{E}\{(\boldsymbol{h}(\boldsymbol{x}) - \boldsymbol{m}_h^{(\ell,\cdot)})(\boldsymbol{h}(\boldsymbol{x}) - \boldsymbol{m}_h^{(\ell,\cdot)})^T\} \,, \tag{9c}$$

where the expectations are taken with respect to $p_g(\boldsymbol{x}; \boldsymbol{m}_x^{(\ell,\cdot)}, \boldsymbol{P}_{xx}^{(\ell,\cdot)})$. Equations (7)-(9) define the general architecture for the discrete parameter flow filter using Gaussian mixtures. Recall that the Gaussian case is recovered by having a single GMM component. Of note is the similarity to the original GMM filtering equations[12]. Effectively, Equations (7)-(9) describe an iteration of the GMM filtering equations for M increments Δs_m, which makes the implementation of these equations for existing GMM filters straightforward. The proof of Equations (7) is given in Appendix A of Reference 14.

Variations of Filter Formulation

The expectations of Equations (9) can be handled in a variety of ways. The most common approach is to approximate them as first order Taylor series expansions about the component mean at the current pseudotime step; that is,

$$\begin{aligned}
\boldsymbol{m}_h^{(\ell,i-1)} &\approx \boldsymbol{h}(\boldsymbol{m}_x^{(\ell,i-1)}) \\
\boldsymbol{P}_{xh}^{(\ell,i-1)} &\approx \boldsymbol{P}_{xx}^{(\ell,i-1)} (\boldsymbol{H}_x^{(\ell,i-1)})^T \\
\boldsymbol{P}_{hh}^{(\ell,i-1)} &\approx \boldsymbol{H}_x^{(\ell,i-1)} \boldsymbol{P}_{xx}^{(\ell,i-1)} (\boldsymbol{H}_x^{(\ell,i-1)})^T \,,
\end{aligned}$$

where $\boldsymbol{H}_x^{(\ell,i-1)}$ is the Jacobian of $\boldsymbol{h}(\boldsymbol{x})$ with respect to $\boldsymbol{x}$, evaluated at $\boldsymbol{m}_x^{(\ell,i-1)}$. An implementation of Equations (7)-(9) with these Taylor series approximations is referred to as the discrete parameter flow extended Gaussian mixture filter (DPF-EGMF).

Alternatively, one may consider a set of N_q weights and points that comprise a quadrature rule for expectations with respect to $p_g(\boldsymbol{x}; \boldsymbol{m}_x^{(\ell,i-1)}, \boldsymbol{P}_{xx}^{(\ell,i-1)})$ of the form $\{w_m^{(\ell,j)}, w_c^{(\ell,j)}, \boldsymbol{\mathcal{X}}^{(\ell,i-1,j)}\}_{j=0}^{N_q-1}$. These weights and points are constructed such that

$$\begin{aligned}
\boldsymbol{m}_x^{(\ell,i-1)} &= \sum_{j=0}^{N_q-1} w_m^{(\ell,j)} \boldsymbol{\mathcal{X}}^{(\ell,i-1,j)} \\
\boldsymbol{P}_{xx}^{(\ell,i-1)} &= \sum_{j=0}^{N_q-1} w_c^{(\ell,j)} (\boldsymbol{\mathcal{X}}^{(\ell,i-1,j)} - \boldsymbol{m}_x^{(\ell,i-1)})(\boldsymbol{\mathcal{X}}^{(\ell,i-1,j)} - \boldsymbol{m}_x^{(\ell,i-1)})^T .
\end{aligned}$$

Note that the quadrature weights carry no dependence on i; that is, the quadrature scheme is taken to have constant weights through the update, which is common. The quadrature-based approximation of the expected values of Equations (9) that are required for the discrete parameter flow approach are then given by

$$\begin{aligned}
\boldsymbol{m}_h^{(\ell,i-1)} &\approx \sum_{j=0}^{N_q-1} w_m^{(\ell,j)} \boldsymbol{h}(\boldsymbol{\mathcal{X}}^{(\ell,i-1,j)}) \\
\boldsymbol{P}_{xh}^{(\ell,i-1)} &\approx \sum_{j=0}^{N_q-1} w_c^{(\ell,j)} (\boldsymbol{\mathcal{X}}^{(\ell,i-1,j)} - \boldsymbol{m}_x^{(\ell,i-1)})(\boldsymbol{h}(\boldsymbol{\mathcal{X}}^{(\ell,i-1,j)}) - \boldsymbol{m}_h^{(\ell,i-1)})^T \\
\boldsymbol{P}_{hh}^{(\ell,i-1)} &\approx \sum_{j=0}^{N_q-1} w_c^{(\ell,j)} (\boldsymbol{h}(\boldsymbol{\mathcal{X}}^{(\ell,i-1,j)}) - \boldsymbol{m}_h^{(\ell,i-1)})(\boldsymbol{h}(\boldsymbol{\mathcal{X}}^{(\ell,i-1,j)}) - \boldsymbol{m}_h^{(\ell,i-1)})^T .
\end{aligned}$$

An implementation of Equations (7)-(9) with these approximations is referred to as the discrete parameter flow quadrature Gaussian mixture filter (DPF-QGMF). Several quadrature rules are available for implementation, such as Gauss-Hermite quadrature[15] and the unscented transform[16]. An implementation using the unscented transform is herein referred to as the discrete parameter flow unscented Gaussian mixture filter (DPF-UGMF).

Almost all quadrature rules generate points $\boldsymbol{\mathcal{X}}^{(\cdot)}$ using square-root factors (SRFs) of the covariance matrix. Factorized versions of sequential filters are ubiquitous in operational settings due to their increased numerical stability[17]. To that end, it is beneficial to construct a variation of Equations (7)-(9) that rely on SRFs. Let $\boldsymbol{S}_{aa}$ be an SRF, where $\boldsymbol{S}_{aa}\boldsymbol{S}_{aa}^T = \boldsymbol{P}_{aa}$ for a random vector $\boldsymbol{a}$. Expressing all covariance matrices in Equation (7c) by their SRFs and factoring out the gain gives

$$\boldsymbol{S}_{xx}^{(\ell,i)}(\boldsymbol{S}_{xx}^{(\ell,i)})^T = \boldsymbol{S}_{xx}^{(\ell,i-1)}(\boldsymbol{S}_{xx}^{(\ell,i-1)})^T - \boldsymbol{K}^{(\ell,i-1)} \left[\boldsymbol{S}_{hh}^{(\ell,i-1)}(\boldsymbol{S}_{hh}^{(\ell,i-1)})^T + \frac{1}{\Delta s_i} \boldsymbol{S}_{vv}\boldsymbol{S}_{vv}^T \right] (\boldsymbol{K}^{(\ell,i-1)})^T .$$

The SRF $\boldsymbol{S}_{vv}$ is typically stored *a priori*; however, $\boldsymbol{S}_{hh}^{(\ell,i-1)}$ is constructed differently depending on the method of choice for computing expectations. Both factorized implementations are developed herein for completeness. Starting from the previous state SRF $\boldsymbol{S}_{xx}^{(\ell,i-1)}$, the linearized implementa-

tion results in

$$\boldsymbol{S}_{hh}^{(\ell,i-1)} = \boldsymbol{H}_{x}^{(\ell,i-1)} \boldsymbol{S}_{xx}^{(\ell,i-1)} \,.$$

Within the quadrature implementation, there are a variety of approaches to compute $\boldsymbol{S}_{hh}^{(\ell,i-1)}$. However, care must be taken since it may be the case that one or more of the covariance weights $w_c^{(\ell,j)}$ is negative. A straightforward method, taken from Reference 18, is to sort the weights such that the first r weights are negative, and the remaining $N_q - r$ weights are positive. Then, define the weight matrix

$$\boldsymbol{W}^{(\ell)} \triangleq \text{diag}\left\{ \sqrt{|w_c^{(\ell,1)}|}, \ldots, \sqrt{|w_c^{(\ell,r)}|}, \sqrt{w_c^{(\ell,r+1)}}, \ldots, \sqrt{w_c^{(\ell,N_q)}} \right\} ,$$

where $\text{diag}\{\cdot\}$ denotes a diagonal concatenation. Let $\boldsymbol{W}^{(\ell,p:q)}$ be the square submatrix of $\boldsymbol{W}^{(\ell)}$ containing the p^{th} to q^{th} rows and columns of $\boldsymbol{W}^{(\ell)}$. Additionally, let $\boldsymbol{\mathcal{X}}^{(\ell,i-1,p:q)}$ be a column-wise concatenation of the p^{th} to q^{th} quadrature points. Then, the SRF $\boldsymbol{S}_{hh}^{(\ell,i-1)}$ is computed by*

$$\begin{aligned} \boldsymbol{M}^{(\ell)} &= \text{qr}\left\{ (\boldsymbol{h}(\boldsymbol{\mathcal{X}}^{(\ell,i-1,r+1:N_q)}) \ominus \boldsymbol{m}_h^{(\ell,i-1)}) \boldsymbol{W}^{(\ell,r+1:N_q)} \right\} \\ \boldsymbol{S}_{hh}^{(\ell,i-1)} &= \text{cholupdate}\{\boldsymbol{M}^{(\ell)}, (\boldsymbol{h}(\boldsymbol{\mathcal{X}}^{(\ell,i-1,1:r)}) \ominus \boldsymbol{m}_h^{(\ell,i-1)}) \boldsymbol{W}^{(\ell,1:r)}, \text{“}-\text{”}\} \,, \end{aligned}$$

where $\text{qr}\{\cdot\}$ represents the QR-decomposition as used in Reference 19, $\text{cholupdate}\{\boldsymbol{A}, \boldsymbol{B}\}$ denotes the Cholesky update[20] of $\boldsymbol{A}$ by $\boldsymbol{B}$, and "$-$" indicates a Cholesky downdate†

Once $\boldsymbol{S}_{hh}^{(\ell,i-1)}$ is acquired either by linearization or quadrature, computing the updated state SRF $\boldsymbol{S}_{xx}^{(\ell,i)}$ necessitates, in order, a rank-m Cholesky update and a rank-m Cholesky downdate, where m is the size of the measurement vector. The complete update is given by

$$\boldsymbol{S}_{zz}^{(\ell,i-1)} = \text{cholupdate}\{\boldsymbol{S}_{hh}^{(\ell,i-1)}, \frac{1}{\sqrt{\Delta s_i}} \boldsymbol{S}_{vv}\} \tag{13a}$$

$$\boldsymbol{S}_{xx}^{(\ell,i)} = \text{cholupdate}\{\boldsymbol{S}_{xx}^{(\ell,i-1)}, \boldsymbol{K}^{(\ell,i-1)} \boldsymbol{S}_{zz}^{(\ell,i-1)}, \text{“}-\text{”}\} \,. \tag{13b}$$

The prediction stage for a square-root factorized sequential filter operating on Equation (1a) is not the subject of this paper, but the equations can be found in Reference 19.

Adaptive Selection of Discrete Pseudotime Steps

An important question for the discrete parameter flow approach is how to select the pseudotime increments Δs_m. There are two tuning parameters: (i) the number of increments M and (ii) the size of the increments relative to one another. The simplest approach is to fix M and use equal increments. Constant (or a maximum allowable) M results in a fixed computational burden and that is the approach taken herein. For the relative sizes of the increments, one can consider an optimization approach such as the one used in Reference 14, though solving a nonlinear optimization problem at every inference step introduces an inconsistent computational overhead. It is also important to consider that $\boldsymbol{P}_{vv}/\Delta s_m \to \infty$ as $\Delta s_m \to 0$ and numerical issues may arise. There may also be many instances where a single step inference performs nearly identically to a multi-step one—especially when the *a priori* state uncertainty and measurement precision are similarly sized.

*The shorthand notation $\boldsymbol{A} \ominus \boldsymbol{a}$ denotes that the vector $\boldsymbol{a}$ is subtracted from each column of the matrix $\boldsymbol{A}$.

†This notation is aligned with the MATLAB function `cholupdate`.

In light of the aforementioned points, this work introduces an adaptive approach that balances computational expediency and inference robustness. Instead of a fixed set of steps for all inference phases, a maximum step amount M_{max} is prescribed along with a minimum step size ε. For the ℓ^{th} GMM component, the step size at instance m is computed via

$$s_m^{(\ell)} = \left(\frac{\|\boldsymbol{S}_{vv}\|}{\|\boldsymbol{S}_{hh}^{(\ell,m)}\|} \right)^2, \tag{14}$$

so as to enforce that $\|\boldsymbol{S}_{hh}^{(\ell,i)}\|$ and $\|\boldsymbol{S}_{vv}/\sqrt{s_i^{(\ell)}}\|$ are identical. The norm $\|\cdot\|$ is taken to be the spectral norm. As the inference phase progresses, the cumulative step amount taken $\bar{s}$ is also tracked where $\bar{s} = 0$ at $m = 1$. Steps given by Equation (14) are taken unless (i) the computed value for $s_m^{(\ell)}$ is greater than $1 - \bar{s}$, then $s_m^{(\ell)} = 1 - \bar{s}$, (ii) the maximum number of steps is reached, or (iii) the computed value for $s_i^{(\ell)}$ is less than ε, then $s_m^{(\ell)} = \varepsilon$. Pseudocode for the adaptive inference phase is illustrated through Algorithim 1. A GMM filter implementation which uses this method for increments is denoted as an ADPF-GMF.

Algorithm 1 ADPF-GMF Step Selection

Require: $\boldsymbol{S}_{hh}^{(\ell,i)}$, $\boldsymbol{S}_{vv}$, M_{max}, ε
Initialize: $\bar{s} = 0$, $m = 1$
while $\bar{s} < 1$ **and** $m < M_{\text{max}}$ **do**
    $\boldsymbol{s}_m^{(\ell)} \leftarrow$ Equation 14
    if $\boldsymbol{s}_m^{(\ell)} \geq 1 - \bar{s}$ **then**
        $\boldsymbol{s}_m^{(\ell)} \leftarrow 1 - \bar{s}$
    else if $s < \varepsilon$ **then**
        $s \leftarrow \varepsilon$
    end if
    if $\boldsymbol{s}_m^{(\ell)} < 1 - \bar{s}$ **and** $m = M_{\text{max}}$ **then**
        $\boldsymbol{s}_m^{(\ell)} \leftarrow 1 - \bar{s}$
    end if
    Update using Equations (13)
    $m++$ and $\bar{s} = \bar{s} + \boldsymbol{s}_m^{(\ell)}$
end while
Repeat for all GMM components

DEMONSTRATION

To demonstrate the capability of the discrete parameter flow filter, a simplified two-dimensional Monte Carlo analysis is presented. A GMM pdf representing the true prior $p(\boldsymbol{x}_k)$ is constructed for a state $\boldsymbol{x} = [x, y]^T$ and illustrated in Figure 1. A set of 1,000 precise, highly-informative measurements is generated from a tail sample at $\boldsymbol{x}_{\text{tail}} = [44, 10]^T$ of the GMM prior, which is also shown in Figure 1. The units for $\boldsymbol{x}$ are taken to be generic distance units. The measurement includes range and bearing modeled as $\boldsymbol{z} = [\|\boldsymbol{x}\|, \tan^{-1}(y/x)]^T + \boldsymbol{v}$ where $\boldsymbol{v}$ is zero-mean, Gaussian with covariance $\boldsymbol{P}_{vv} = \text{diag}([2.5 \times 10^{-5}, 0.5^2 \text{ arcsec}^2])$.

The objective is to compare various filter correctors on a dispersion of precise measurements with low probability. The performance of the different correctors considered in this analysis is analyzed

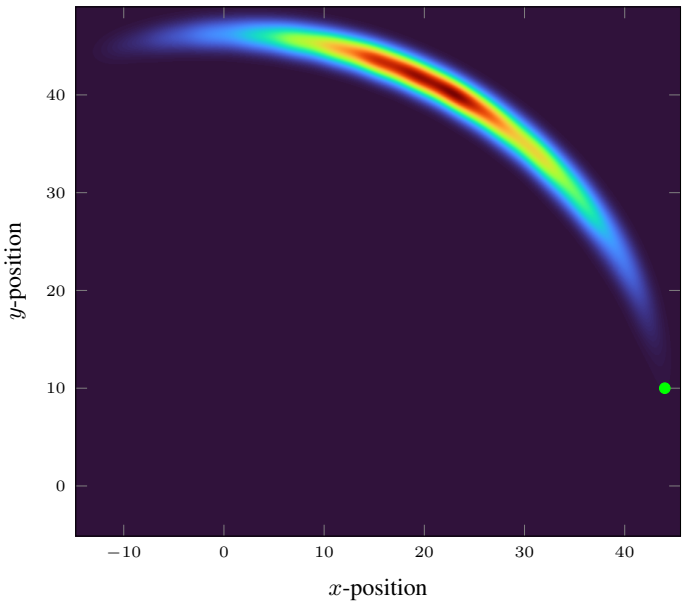

Figure 1. Prior pdf with truth sample at the tail (●)

using the norm of the posterior estimation error, $\boldsymbol{e}_x^+$,

$$\|\boldsymbol{e}_x^+\| = \|\boldsymbol{x} - \boldsymbol{m}_x^+\|\,,$$

and the normalized estimation error squared (NEES),

$$d = \frac{1}{n}(\boldsymbol{x} - \boldsymbol{m}_x^+)^T(\boldsymbol{P}_{xx}^+)^{-1}(\boldsymbol{x} - \boldsymbol{m}_x^+)\,,$$

where $n = 2$ is the state dimension, $\boldsymbol{m}_x^+$ is the posterior mean (the estimate), and $\boldsymbol{P}_{xx}^+$ is the posterior covariance. A well-behaved filter corrector produces an accurate posterior (i.e., the error norm is near zero) and is statistically consistent (i.e., the mean NEES is near one). Six filters are compared and are binned into two groups of three: one group uses Taylor series linearization to approximate Equations (9) (i.e., "extended" filters) and the other group uses the unscented transform quadrature rule (i.e., "unscented" filters) with parameters $\alpha = 0.1$, $\beta = 2$, and $\kappa = 1$ [16]. Within each group, the three filters are (i) a Kalman filter (EKF/UKF) with Gaussian prior consisting of mean and covariance matched to the true prior, (ii) a Gaussian mixture filter (EGMF/UGMF) with prior matching the truth, and (iii) a discrete parameter flow Gaussian mixture filter (DPF-EGMF/DPF-UGMF) with prior matching the truth. For the discrete parameter flow filters, a set of $M = 40$ steps in pseudotime is applied via a cubic rule. Importantly, the EKF/UKF filters are given the ability to underweight the measurements by a factor of $p = 0.7$ for added robustness [17].

The norm of the posterior estimation errors and the NEES values for the six filters are illustrated in Figures 2-5 as box plots. The box plot includes the median of the data as the red mark within the box. The box itself depicts data residing within the 25^{th} and 75^{th} percentiles. The dashed lines extending from the box illustrate the extent of the most extreme data points. The Gaussian filters (EKF/UKF) produce ill-behaved posteriors for all MC trials, even with underweighting applied. This is primarily due to a poor representation of the prior pdf in the inference procedure, reiterating the need for enhanced uncertainty realism. Despite applying an underweighting factor of $p = 0.7$,

the EKF/UKF posteriors possess poor statistical consistency. The EGMF/UGMF filters present an improvement over the Kalman filters; however, they suffer from significant overconfidence as indicated by median NEES values greater than two (see Figure 5). Trials that produce the most overconfident posteriors reach a NEES of nearly seven for the EGMF. Although the EGMF/UGMF start out with a perfect prior pdf, there are many components in the GMM that perform a large single-step update—resulting in inconsistency.

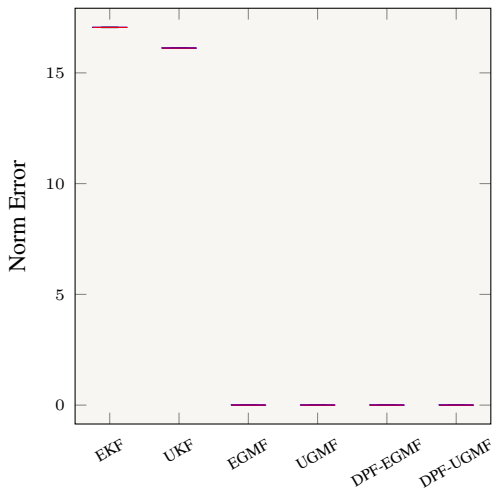

Figure 2. Norm of posterior estimation errors from demonstration example.

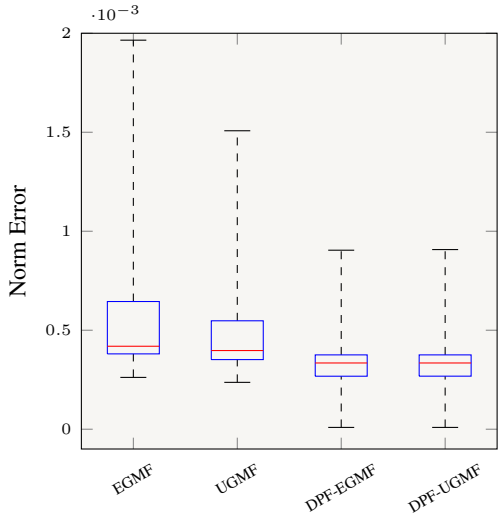

Figure 3. Norm of posterior estimation errors from demonstration example (zoomed).

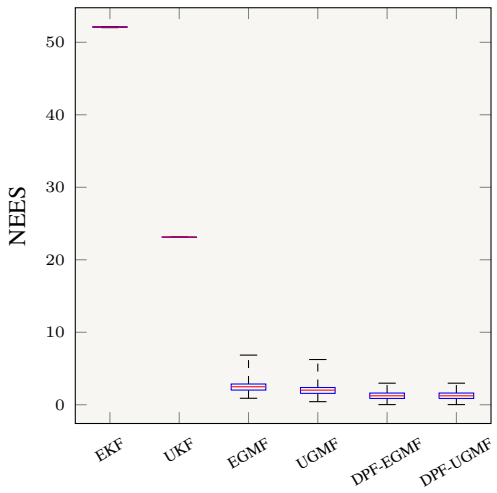

Figure 4. NEES measure for posterior estimates.

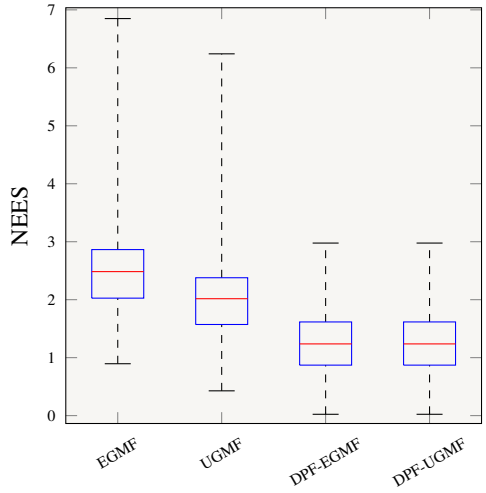

Figure 5. NEES measure for posterior estimates (zoomed).

In contrast, the DPF-EGMF/DPF-UGMF filters illustrate a well-behaved inference procedure, with a 50% decrease in worst-case error and a median NEES near one. The most overconfident posteriors from discrete parameter flow are half as overconfident as their single-step counterparts (see Figure 5). An interesting result is that, for this demonstration, the discrete parameter flow filters

have negligible differences in norm error and NEES values despite their difference in method for approximating Equations (9). Since $M = 40$ steps are taken, it is likely that the steps are small enough such that statistical and analytical linearization yield nearly identical performance.

CISLUNAR SPACE OBJECT TRACKING

The goal for any sequential filter is to produce accurate and statistically consistent estimates over time. Moreover, in the context of space object tracking, the filter must maximize information extraction from potentially sparse measurement sets. To that end, this section demonstrates the statistical estimation performance of discrete parameter flow via Monte Carlo (MC) analysis for a cislunar orbit.

Simulation and Filtering Description

Three filters with configurations described in Table 1 are used to process measurements for an object in an Elliptical Lunar Frozen Orbit (ELFO). The initial conditions for the ELFO are detailed in Table 2 with a single period of the ELFO illustrated in Figure 6. All filters have a state vector comprised of the satellite's position $\boldsymbol{r}$ and velocity $\boldsymbol{v}$ expressed in the Earth-centered J2000 inertial frame.[21]

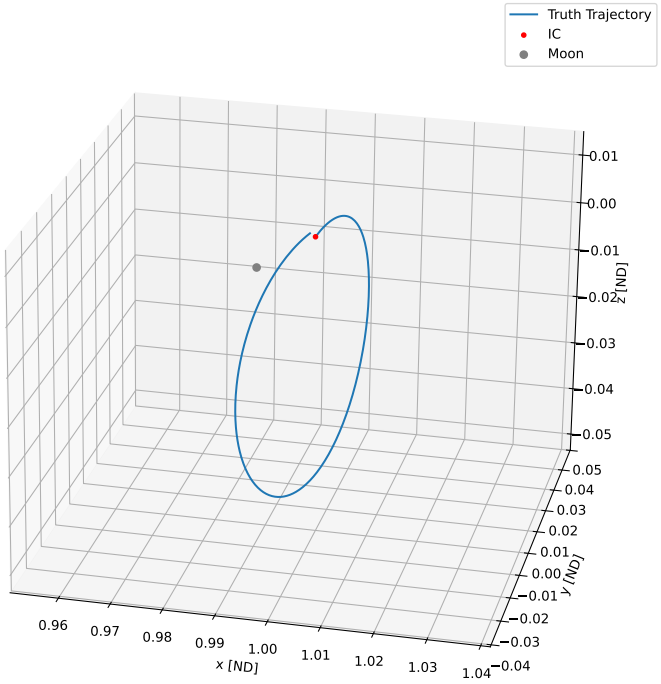

Figure 6. Single period of the ELFO in the Earth-Moon rotating frame with ND $= 384,487$ km. One period is about 1.3 days.

Table 1. Filter configurations. All filters use the linearized, square-root factor implementation.

Name	Step Size Method
EGMF	Single Step
DPF-EGMF	Linear Steps $M = 30$
ADPF-EGMF	Adaptive Steps $M_{\max} = 30$

Table 2. ELFO initial states and covariance SRF for epoch Jan 6 2027. Units are given in km and km/s. `blkdiag` denotes a block diagonal concatenation.

$\boldsymbol{m}_0$	$\boldsymbol{S}_0$
[-58957, -355755, -184811, 2.081, -0.872, 2.132]^T	$\texttt{blkdiag}(0.1 \cdot \boldsymbol{I}_3, 10^{-6} \cdot \boldsymbol{I}_3)$

Dynamics Modeling The dynamics model used by both the truth and within the filters is a point-mass, ephemeris model given by

$$\begin{aligned}\dot{\boldsymbol{r}} &= \boldsymbol{v} \\ \dot{\boldsymbol{v}} &= \boldsymbol{a}_g + \sum_{i=1}^{I} \boldsymbol{a}_{3\text{rd},i}\,,\end{aligned}$$

where $\boldsymbol{a}_g$ is the central body (Earth) gravity and $\boldsymbol{a}_{3\text{rd},i}$ is the third-body gravity perturbation for the i^{th} mass[21]. The two third-body masses used in this analysis are the Moon and Sun—with their positions determined using SPICE[22]. Letting $\boldsymbol{f} = [\dot{\boldsymbol{r}}^T\ \dot{\boldsymbol{v}}^T]^T$, each GMM component mean $\boldsymbol{m}_x^{(\ell)}$ and state transition matrix $\boldsymbol{\Phi}_x^{(\ell)}$ is propagated from the previous measurement to the next one according to

$$\begin{aligned}\dot{\boldsymbol{m}}_x^{(\ell)} &= \boldsymbol{f}(\boldsymbol{m}_x^{(\ell)}) \\ \dot{\boldsymbol{\Phi}}_x^{(\ell)} &= \boldsymbol{F}(\boldsymbol{m}_x^{(\ell)})\boldsymbol{\Phi}_x^{(\ell)}\,,\end{aligned}$$

where $\boldsymbol{F}(\boldsymbol{m}_x^{(\ell)})$ is the Jacobian of $\boldsymbol{f}(\cdot)$ evaluated at the component mean $\boldsymbol{m}_x^{(\ell)}$, and the initial conditions are $\boldsymbol{m}_x^{(\ell)}(t_{k-1}) = \boldsymbol{m}_{x,k-1}^{(\ell)}$ and $\boldsymbol{\Phi}_x^{(\ell)}(t_{k-1}) = \boldsymbol{I}_n$. The result of integrating the previous ODEs is an *a priori* mean $\boldsymbol{m}_{x,k}^{(\ell)}$ and state transition matrix $\boldsymbol{\Phi}_{x,k}^{(\ell)}$. The GMM component covariance SRF $\boldsymbol{S}_{xx}^{(\ell)}$ is then propagated via

$$\boldsymbol{S}_{xx,k}^{(\ell)} = \boldsymbol{\Phi}_{x,k}^{(\ell)}\boldsymbol{S}_{xx,k-1}^{(\ell)}\,.$$

Moon-based Line-of-Sight The Moon-based line-of-sight (LOS) measurements are generated by an observer fixed to the center of the Moon. A center-Moon observer is chosen to avoid fixed frame transformations. The values for the Moon observer are identical to the Moon positions generated from SPICE for the dynamics modeling. The model used for both the true measurements and the filter inference phase is

$$\boldsymbol{z} = \begin{bmatrix}\alpha \\ \beta\end{bmatrix} = \begin{bmatrix}\tan^{-1}(\frac{y}{x}) \\ \tan^{-1}(z/\sqrt{x^2+y^2})\end{bmatrix} + \boldsymbol{v}\,,$$

where x, y, and z are the components of the vector $\boldsymbol{r} - \boldsymbol{r}_{\text{obs}}$ and $\boldsymbol{v}$ is a zero-mean, uncorrelated, Gaussian noise with standard deviations of 3 arcseconds for α and β.

Filtering Description The three filters compared in this scenario—outlined in Table 1—all use the same GMM for the initial state PDF. The GMM is created using an optimized splitting library[23] that approximates the initial Gaussian for each orbit defined using $L = 27$ GMM components. These components are generated by splitting the initial Gaussian recursively among each velocity component. Each filter is given identical measurement sets across all times for consistency. The DPF-EGMF uses linear steps for inference, meaning that each consecutive step increases linearly. The ADPF-EGMF uses Algorithm 1 for computing its steps, with a maximum number of allowable steps equal to the DPF-EGMF step configuration.

Results and Discussion

The 27-component GMM is propagated from the initial epoch to one, two, and three orbital periods. A single period of the ELFO is shown in Figure 6. At each orbital period, 1000 samples are generated from the GMM to compute a set of line-of-sight measurements. Each filter configuration then processes this same set of measurements to create 1000 posterior GMMs. This is repeated for two and three orbital periods prior to measurement generation. The truth samples are generated from the propagated GMM in order to isolate the inference phase from the uncertainty propagation phase.

The statistical performance of all three filter implementations after propagating one orbital period and processing a single line-of-sight measurement is given in Figures 7-9 for the x-y position states. The average filter $\pm 3\sigma$ corresponds to the 99.5% intervals of the average posterior pdf covariance. The single step EGMF fails to provide an unbiased solution, as seen by the nonzero average error from the trial ensemble. Further, the average filter uncertainty markedly fails to capture the distribution of the error ensemble in both size and shape. In contrast, the DPF-EGMF and ADPF-EGMF in Figures 8 and 9 result in statistically unbiased performance with an accurate characterization of the true underlying error distribution (the average filter $\pm 3\sigma$ aligns with that approximated by Monte Carlo). Note that the axes scaling is identical in Figures 7-9, highlighting the ability of the multi-step inference procedure to produce precise posteriors. Importantly, though the DPF-EGMF and ADPF-EGMF yield nearly identical statistical performance, the ADPF-EGMF uses almost *half of the steps* as its pre-determined steps counterpart (16 instead of 30). Similar estimation performance occurs for the other spacecraft states and is omitted here for brevity.

The root sum-of-squares (RSS) of the position errors for each filter across the three orbital periods where measurements are processed are shown in Figures 10-12 via box plots. The axes are scaled identically for each filter for consistent comparison. The multi-step filters have median errors of the same amount (≈ 120 meters) when processing a single measurement after three orbits as the single-step filter has for processing a measurement after one orbit. Notably, for processing a measurement after three orbits, the ADPF-EGMF presents improved worst-case-error behavior due to the ability to take smaller steps than a designer can *a priori* optimize. This added robustness also *costs less* by measure of number of steps taken compared to the $M = 30$ steps taken by the DPF-EGMF. The number of steps taken by each GMM component of the ADPF-EGMF, for each measurement processing epoch, is depicted in Figure 13. Interestingly, for a given amount of propagation before the measurement, each GMM component takes the same number of inference steps regardless of the measurement value.

As important as unbiased performance is statistical consistency of the filter. To evaluate consistency, the NEES measure used in the 2D demonstration is reused here, now with state dimension $n = 6$. Recall a NEES above unity indicates an overconfident posterior, while a NEES below unity

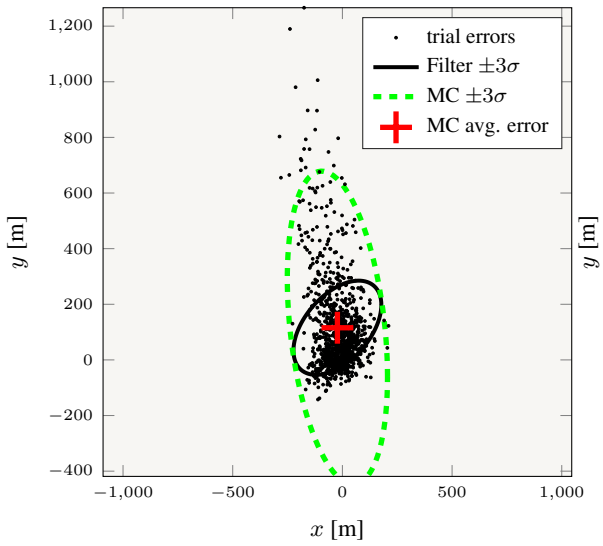

Figure 7. EGMF x-y statisical performance after one period.

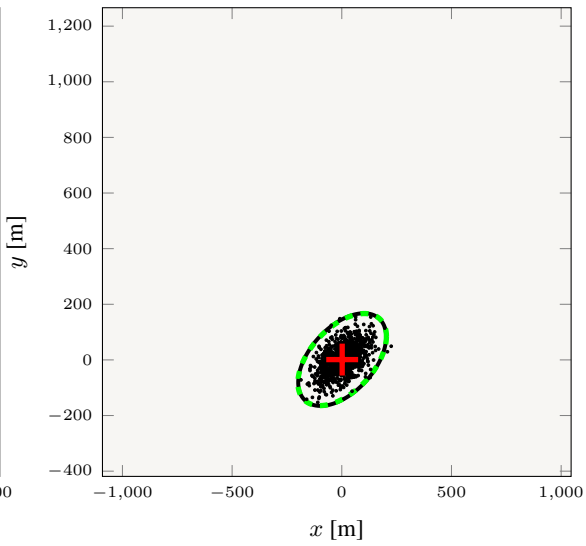

Figure 8. DPF-EGMF x-y statisical performance after one period.

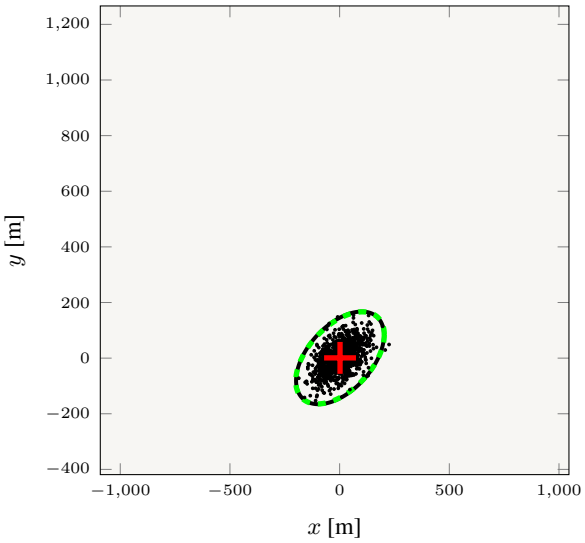

Figure 9. ADPF-EGMF x-y statisical performance after one period.

indicates a conservative one. The NEES values for the filters are illustrated in Figures 14-16. Even after just one orbital period of propagation, the median EGMF posterior estimate is statistically overconfident and grows significantly moreso as the propagation period increases. Conversely, both the DPF-EGMF and ADPF-EGMF retain a median posterior that is slightly conservative regardless of the amount of propagation before processing the measurement. The ADPF-EGMF also exhibits improved consistency in tail (i.e., low probability) cases when propagating three orbit periods before processing a measurement, as seen in Figure 16. The superior outlier performance of the ADPF-EGMF is due to the ability to adaptively take small steps in the first partitions of the inference phase.

This specific ELFO analysis, though highly constrained, demonstrates the potential for significant

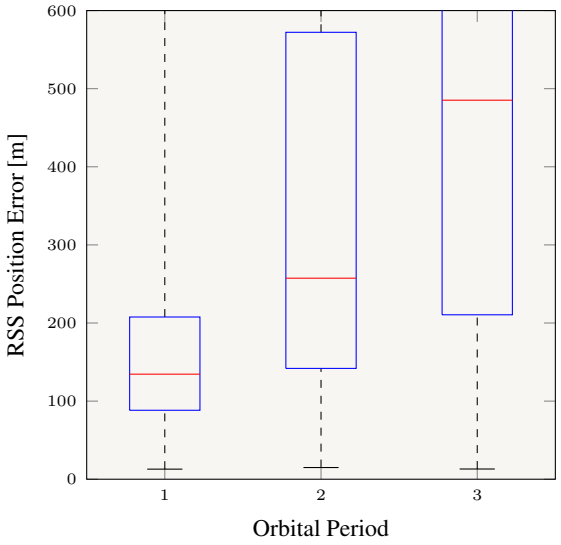

Figure 10. EGMF.

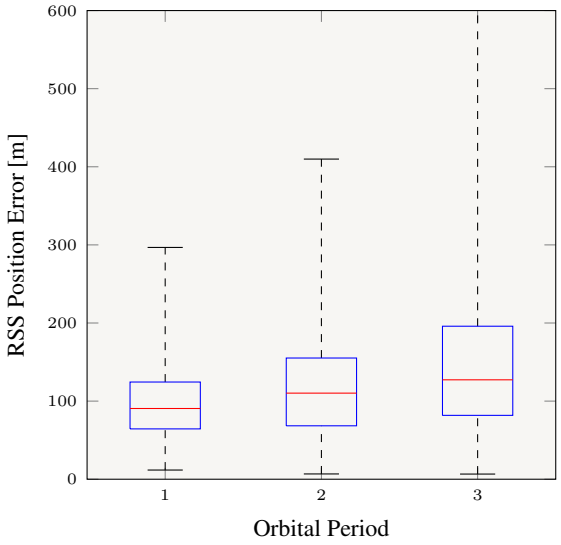

Figure 11. DPF-EGMF.

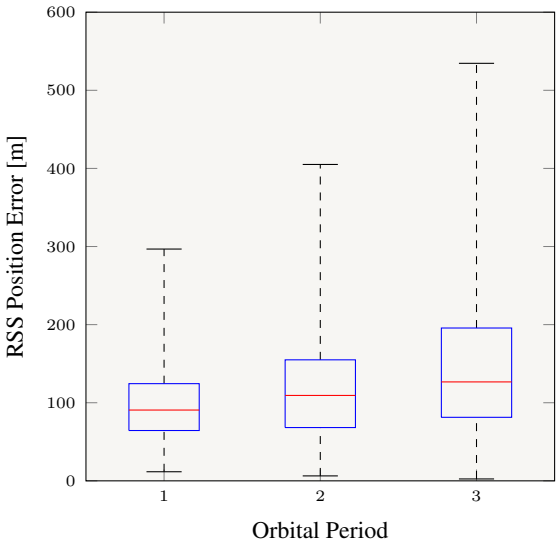

Figure 12. ADPF-EGMF

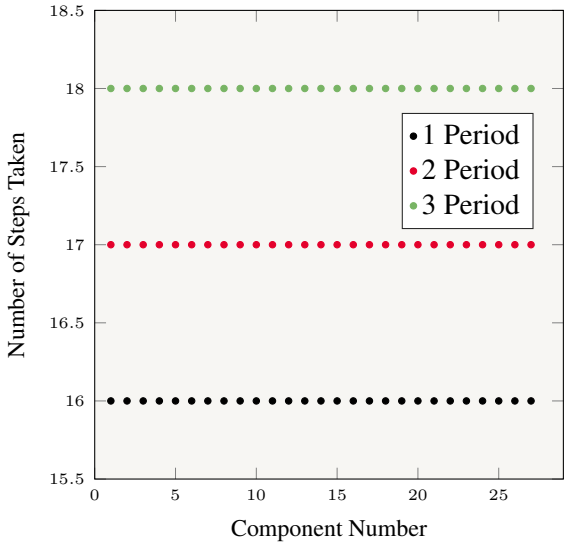

Figure 13. Measurement inference steps taken by the ADPF-EGMF for each orbital period before measurement processing. Maximum allowable steps is 30.

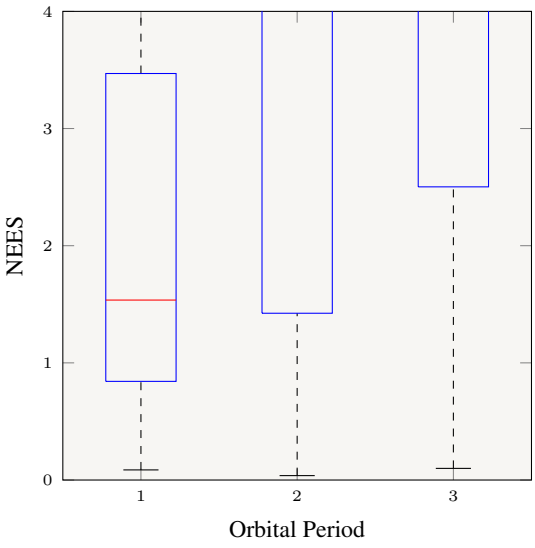

Figure 14. EGMF.

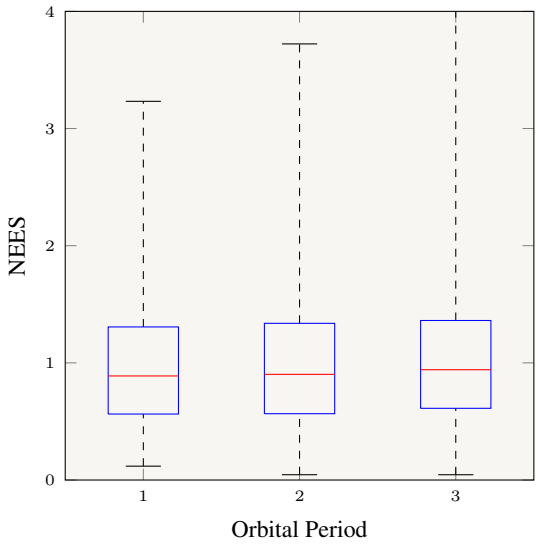

Figure 15. DPF-EGMF.

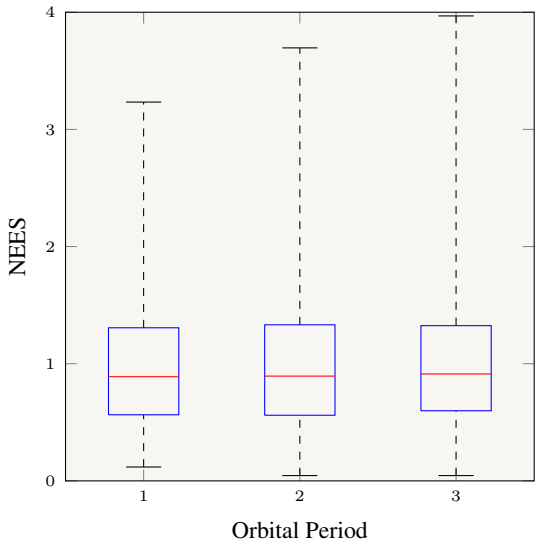

Figure 16. ADPF-EGMF

operational savings enabled by the discrete parameter flow procedure—particularly through its ability to achieve similar estimation performance to that of a traditional single-step inference method even with *longer period beetween measurements*. This capability arises from two key features of discrete parameter flow. First, by partitioning the measurement update, a fundamentally nonlinear inference step can be well approximated by a sequence of small linear ones. Second, as a consequence of this partitioning, the tail portions of the prior pdf are preserved more effectively than in single-step inference, where they are more easily discarded.

CONCLUSIONS

There are numerous challenges faced when conducting recursive Bayesian inference for nonlinear systems—especially when measurement information is sparsely available. Many approaches attempt to overcome this problem through better uncertainty quantification (e.g., Gaussian mixture propagation), *ad hoc* robustness techniques (e.g., underweighting), or by over-observing the system. Alternatively, this work proposes a discrete homotopic continuation of Bayes' rule, termed discrete parameter flow, that partitions the traditional single-step update into multiple incremental updates. The motivation for this partitioned approach is that approximations made in the inference procedure are dampened by taking small steps from prior to posterior. Multiple variations of discrete parameter flow are presented including a square-root factorized version for increased numerical stability. Additionally, a novel algorithm for adaptive step size selection is presented. This adaptive step procedure aims to ameliorate the problem of deciding the best step size profile for any specific filter implementation.

On a simplified scenario, the approach is shown to provide superior performance when traditional filtering schemes fail. The simplified scenario highlights how discrete parameter flow can make use of a highly-informative observation—especially when the prior state uncertainty is large. These findings are also observed in a cislunar tracking scenario, wherein traditional schemes fail at processing a single line-of-sight measurement after one or more orbital periods of uncertainty growth while discrete parameter flow yields unbiased and statistically consistent posterior estimates. Moreover, the filters leveraging adaptive step size selection for inference achieve similar to improved

performance but with less steps (half in the analysis herein) taken than their fixed-step counterparts. This adaptive procedure keeps the filter from taking an unnecessary amount of steps, amounting to savings in computational runtime.

REFERENCES

[1] R. Strasse, "ESA's Annual Space Environment Report," 2024. Accessed: 2025-03-29.

[2] S. Särkkä and L. Svensson, *Bayesian Filtering and Smoothing*, Vol. 17. Cambridge University Press, 2023.

[3] U. D. Hanebeck, K. Briechle, and A. Rauh, "Progressive Bayes: A New Framework for Nonlinear State Estimation," *Multisensor, Multisource Information Fusion: Architectures, Algorithms, and Applications*, Vol. 5099, SPIE, 2003, pp. 256–267.

[4] F. Daum and J. Huang, "Particle Degeneracy: Root Cause and Solution," *Signal Processing, Sensor Fusion, and Target Recognition XX*, Vol. 8050, SPIE, 2011, pp. 367–377.

[5] K. C. Ward and K. J. DeMars, "Information-Based Particle Flow With Convergence Control," *IEEE Transactions on Aerospace and Electronic Systems*, Vol. 58, No. 2, 2021, pp. 1377–1390.

[6] R. Zanetti, "Recursive Update Filtering for Nonlinear Estimation," *IEEE Transactions on Automatic Control*, Vol. 57, No. 6, 2011, pp. 1481–1490.

[7] K. Michaelson, A. A. Popov, and R. Zanetti, "Ensemble Kalman Filter with Bayesian Recursive Update," *26th International Conference on Information Fusion (FUSION)*, IEEE, 2023, pp. 1–6.

[8] K. Michaelson, A. A. Popov, R. Zanetti, and K. J. DeMars, "Particle Flow with a Continuous Formulation of the Nonlinear Measurement Update," *27th International Conference on Information Fusion (FUSION)*, IEEE, 2024, pp. 1–8.

[9] K. J. Craft and K. J. DeMars, "Homotopic Gaussian Mixture Filtering for Applied Bayesian Inference," *IEEE Transactions on Automatic Control*, 2025, pp. 1–16, 10.1109/TAC.2025.3530878.

[10] A. H. Jazwinski, *Stochastic Processes and Filtering Theory*. Courier Corporation, 1970.

[11] K. Ito and K. Xiong, "Gaussian Filters for Nonlinear Filtering Problems," *IEEE Transactions on Automatic Control*, Vol. 45, No. 5, 2000, pp. 910–927, 10.1109/9.855552.

[12] D. Alspach and H. Sorenson, "Nonlinear Bayesian Estimation Using Gaussian Sum Approximations," *IEEE Transactions on Automatic Control*, Vol. 17, No. 4, 1972, pp. 439–448, 10.1109/TAC.1972.1100034.

[13] Y. Ho and R. Lee, "A Bayesian Approach to Problems in Stochastic Estimation and Control," *IEEE Transactions on Automatic Control*, Vol. 9, No. 4, 1964, pp. 333–339, 10.1109/TAC.1964.1105763.

[14] K. DeMars and W. Fife, "Adaptive Bayesian Inference for Space Object Tracking," *9th European Conference on Space Debris*, 2025.

[15] I. Arasaratnam, S. Haykin, and R. J. Elliott, "Discrete-Time Nonlinear Filtering Algorithms Using Gauss–Hermite Quadrature," *Proceedings of the IEEE*, Vol. 95, No. 5, 2007, pp. 953–977, 10.1109/JPROC.2007.894705.

[16] S. Julier and J. Uhlmann, "Unscented Filtering and Nonlinear Estimation," *Proceedings of the IEEE*, Vol. 92, No. 3, 2004, pp. 401–422, 10.1109/JPROC.2003.823141.

[17] J. R. Carpenter and C. N. D'Souza, "Navigation Filter Best Practices," Tech. Rep. TP-2018-219822, NASA, 2018.

[18] J. S. McCabe and K. J. DeMars, "Square-Root Consider Filters with Hyperbolic Householder Reflections," *Journal of Guidance, Control, and Dynamics*, Vol. 41, No. 10, 2018, pp. 2098–2111.

[19] K. C. Ward, G. S. Fritsch, J. C. Helmuth, K. J. DeMars, and J. S. McCabe, "Design and Anal-

ysis of Descent-to-Landing Navigation Incorporating Terrain Effects," *Journal of Spacecraft and Rockets*, Vol. 57, No. 2, 2020, pp. 261–277.

[20] G. H. Golub and C. F. Van Loan, *Matrix Computations*. JHU Press, 2013.

[21] D. A. Vallado, *Fundamentals of Astrodynamics and Applications*, Vol. 12. Springer Science & Business Media, 2001.

[22] C. H. Acton, "Ancillary data services of NASA's Navigation and Ancillary Information Facility," *Planetary and Space Science*, Vol. 44, No. 1, 1996, pp. 65–70. Planetary data system, https://doi.org/10.1016/0032-0633(95)00107-7.

[23] K. J. DeMars, R. H. Bishop, and M. K. Jah, "Entropy-Based Approach for Uncertainty Propagation of Nonlinear Dynamical Systems," *Journal of Guidance, Control, and Dynamics*, Vol. 36, No. 4, 2013, pp. 1047–1057, 10.2514/1.58987.